Research Article

Interfacial Activation of Catalytically Inert Au (6.7 nm)–Fe$_3$O$_4$ Dumbbell Nanoparticles for CO Oxidation

Binghui Wu[§], Hai Zhang[§], Cheng Chen, Shuichao Lin, and Nanfeng Zheng (✉)

State Key Laboratory for Physical Chemistry of Solid Surfaces and Department of Chemistry, College of Chemistry and Chemical Engineering, Xiamen University, Xiamen 361005, China

ABSTRACT

Au nanoparticles epitaxially grown on Fe$_3$O$_4$ in Au (6.7 nm)–Fe$_3$O$_4$ dumbbell nanoparticles exhibit excellent stability against sintering, but display negligible catalytic activity in CO oxidation. Starting from various supported Au (6.7 nm)–Fe$_3$O$_4$ catalysts prepared by the colloidal deposition method, we have unambiguously identified the significance of the Au–TiO$_2$ interface in CO oxidation, without any possible size effect of Au. *In situ* thermal decomposition of TiO$_2$ precursors on Au–Fe$_3$O$_4$ was found to be an effective way to increase the Au–TiO$_2$ interface and thereby optimize the catalytic performance of TiO$_2$-supported Au–Fe$_3$O$_4$ dumbbell nanoparticles. By reducing the size of Fe$_3$O$_4$ from 15.2 to 4.9 nm, the Au–TiO$_2$ contact was further increased so that the resulting TiO$_2$-supported Au (6.7 nm)–Fe$_3$O$_4$ (4.9 nm) dumbbell particles become highly efficient catalysts for CO oxidation at room temperature.

KEYWORDS

Gold nanocatalysts, support effect, CO oxidation, Au–Fe$_3$O$_4$, dumbbell nanoparticles

Introduction

Gold nanoparticle-based catalysts, particularly with the particle size of gold less than 10 nm [1–11], have attracted increasing research attention since Haruta discovered the remarkable activity of supported gold nanoparticles in CO oxidation at low temperature [12, 13]. To achieve good catalytic activity and stability, gold nanoparticles are generally loaded on high-surface-area supports [1, 3, 14]. While the particle size of gold nanoparticles is important in optimizing the catalytic activity, the selection of appropriate supports has also been found critical to achieving

high catalytic performance and stability of supported gold nanoparticles. In most cases, the size and support effects are likely to operate simultaneously [14], due to the lack of highly reproducible techniques for the controlled preparation of well-defined gold-nanoparticle catalysts, separation of size and support effects therefore remains a challenge [15, 16]. For example, the importance of the Au–TiO$_2$ interface in CO oxidation over real catalysts has been widely proposed and investigated by comparison of various supported gold nanoparticles or between supported TiO$_2$–supported Au nanoparticles and unsupported gold powder [17–20]. The catalysts which were

---

Address correspondence to nfzheng@xmu.edu.cn

[§] These authors contributed equally to this work.

compared typically had different-sized gold particles. however, such studies do not allow a distinction to be made between the Au–TiO$_2$ support effect and the size effect. There therefore appears to be a lack of consistency in the literature regarding the size and support effects for gold nanocatalysts [16].

Fortunately, the recently developed colloidal deposition method allows the preparation of supported gold nanoparticles with more controllable structural parameters [16, 21–24]. A significant improvement of the colloidal deposition method over previous methods is that pre-made gold nanoparticles are used as the precursors. As a result, the preparation of supported gold nanoparticles with narrow particle size distribution is possible, regardless of the size of the gold nanoparticles and the nature of the support. Using the colloidal deposition method, both pre-made Au and Au–Fe$_3$O$_4$ nanoparticles have been used as the precursors to prepare supported gold nanocatalysts in order to study the support effect in CO oxidation. In these studies, the particle size of the gold nanoparticles employed was mainly ≤ 6 nm. Within this size region, however, facile sintering of the Au nanoparticles frequently occurs [16]. These nanoparticles themselves can possess good catalytic activity for CO oxidation even if deposited on inert supports. For example, carbon-supported 6 nm Au nanoparticles have been found to be highly active for CO oxidation [25]. After simple calcination, Au (3 nm)–Fe$_3$O$_4$ dumbbell particles also displayed excellent activity for CO oxidation, however [24]. Such situations make it extremely difficult to unambiguously identify any support effects responsible for significantly promoting catalysis over supported Au nanoparticles.

The main aim of this work is to identify how the Au–TiO$_2$ interface influences the catalytic activity of TiO$_2$-supported Au nanocatalysts in CO oxidation. To distinguish the support effect from the size effect, Au nanoparticles having the size of ~6.7 nm were selected. When 6.7 nm Au nanoparticles are epitaxially grown on 15.2 nm Fe$_3$O$_4$ nanoparticles to form dumbbell nanoparticles they, if not appropriately supported, exhibit negligible catalytic activity in CO oxidation. Importantly, epitaxial growth on Fe$_3$O$_4$ endows the Au nanoparticles with significant anti-sintering

properties during calcination. Therefore, Au (6.7 nm) –Fe$_3$O$_4$ (15.2 nm) dumbbell nanoparticles serve as an excellent system for us to identify any support effect in catalysis by Au nanoparticles. To first evaluate the importance of the Au–TiO$_2$ interface in the catalysis of CO oxidation, comparison studies were performed on Au (6.7 nm)–Fe$_3$O$_4$ (15.2 nm) particles deposited on various supports. After demonstrating the importance of the Au–TiO$_2$ interface, thermal decomposition of TiO$_2$ precursors was then employed to deposit fine TiO$_2$ nanoparticles on Au–Fe$_3$O$_4$, which helped to increase the contact between Au and TiO$_2$ and promote the catalytic performance. By decreasing the particle size of Fe$_3$O$_4$ from 15.2 to 4.9 nm, we also demonstrate at the end of the article that it is possible to convert TiO$_2$-supported Au (6.7 nm)–Fe$_3$O$_4$ dumbbell particles into catalysts which are highly efficient for CO oxidation at room temperature.

1. Experimental

1.1 Materials

All syntheses were carried out using commercially available reagents. HAuCl$_4$·4H$_2$O was purchased from Sinopharm Chemical Reagent Co. Ltd. *Tert*-butylamine:borane complex (TBAB, 95%), Fe(acac)$_3$, oleylamine (OAm, C$_{18}$ content: 80%–90%), and titanium(IV) isopropoxide (TIPO, 98+%) were purchased from Acros Organics. Oleic acid (OLA) was purchased from Guangdong Xilong Chemical Co. Ltd. CO (99.99%) and N$_2$ (99.999%) were purchased from Linde Gas. All chemicals were used as received without further purification.

1.2 Synthesis of 6.7 nm OAm-capped Au nanoparticles

In a typical synthesis, a precursor solution of chloroform (100 mL), OAm (20 mL), and HAuCl$_4$·4H$_2$O (1 g) was prepared and stirred for 10 min in air at 30 °C. A solution containing 0.8 g (9.2 mmol) of TBAB and OAm (1 mL) in 20 mL of chloroform was mixed by sonication and added to the HAuCl$_4$–OAm mixture. Within 10 s, the solution became deep purple. The mixture was further stirred at 30 °C for 1 h before 60 mL of ethanol were

added. The Au nanoparticles were then collected by centrifugation (8500 rpm, 8 min), washed with ethanol and redispersed in chloroform (100 mL, corresponding to ~5 mg/mL).

1.3 Synthesis of Au (6.7 nm)–Fe₃O₄ (15.2 nm) dumbbell nanoparticles by conventional heating

A solution containing Fe(acac)₃ (70.0 mg), OLA (2.7 mL) and OAm (4.0 mL) in a Schlenk tube was heated to 180 °C within 20 min and aged at 180 °C for 10 min under a flow of N_2. 2 mL of OAm containing 5 mg of Au were then injected into the reaction mixture, followed by the addition of 1.33 mL of OLA. The solution was kept at 180 °C for another 90 min, then heated to 300 °C within 25 min and aged for 20 min. After cooling to room temperature, the particles were separated by adding ethanol, centrifuged, and redispersed into chloroform.

1.4 Synthesis of Au (6.7 nm)–Fe₃O₄ (4.9 nm) dumbbell nanoparticles by microwave heating

6.7 nm Au (5 mg), Fe(acac)₃ (45 mg), 1,2-hexadecanediol (50 mg), OLA (1 mL) and OAm (1.5 mL) were mixed together in a 10-mL microwave vial, sealed and stirred in a 50 °C water bath for at least 2 h before microwave irradiation. The microwave reactions were carried out in a focused single-mode microwave synthesis system (Discover, CEM, USA). The mixture was heated to 130 °C by 100 W of microwave radiation with stirring. After keeping at this temperature for 15 min, the mixture was further heated to 185 °C and aged for 30 min. After cooling to room temperature, the particles were separated by adding ethanol, centrifuged, and redispersed into chloroform.

1.5 Loading Au or Au–Fe₃O₄ nanoparticles on TiO₂, SiO₂ or activated carbon

6.7 nm Au nanoparticles were deposited on a Degussa P25 TiO₂ support to generate supported Au (2.5 wt%) catalysts through the colloidal deposition method. Typically, 1 mL of a colloidal dispersion of OAm-capped gold nanoparticles (5 Au mg/mL chloroform) was first diluted by 9 mL of chloroform to form a solution. 200 mg of TiO₂ powder were then added to the Au solution and stirred for 15 min before the solids were collected by filtration. The resulting

solids were then dried at 100 °C and calcined in air at the desired temperature for 2 h to remove the organic capping agents. A similar process was used to prepare supported Au–Fe₃O₄ catalysts on fumed SiO₂ and activated carbon. In order to remove the organic surfactants, the catalysts were calcined at the desired temperature (350, 450, or 550 °C) in air for 2 h.

1.6 Thermal decomposition of TIPO on Au–Fe₃O₄ nanoparticles

As described above, the Au–Fe₃O₄ dumbbell nanoparticles in our studies were prepared by conventional or microwave heating. After the reaction mixtures were cooled to 50 °C, thermal decomposition of TIPO was performed *in situ* by directly injecting 0.6 mL of TIPO into the mixture. While the mixture obtained by conventional heating was heated to 160 °C and aged for 4 h to complete the reaction, the mixture obtained by microwave heating was heated to 185 °C and aged for 10 min. After the mixtures were cooled to room temperature, the corresponding solids were separated by adding ethanol, followed by centrifugation. The composites were then washed well with ethanol and dried at 100 °C. Before catalysis evaluation, the samples were calcined at different temperatures to remove the organic residues.

1.7 Characterization

Transmission electron microscopy (TEM), including high-resolution TEM (HRTEM) studies, were performed on a Tecnai F-30 high-resolution transmission electron microscope operating at 300 kV. X-ray diffraction (XRD) measurements were recorded on a PANalytical X'pert PRO diffractometer using Cu Kα radiation, operating at 40 kV and 30 mA. TGA traces were obtained on a Q600 SDT thermogravimetric analyzer (TA Instruments) from 30 to 700 °C with heating rate of 10 °C/min and an air flow of 100 mL/min.

1.8 Catalytic experiments

The catalytic reactions were carried out in a continuous flow fixed bed glass reactor with internal diameter of 4 mm. The reactor was heated by an electrical heater controlled by a temperature controller. 5% CO in N_2 at 10 mL/min and air at 40 mL/min

were fed to the reactor by mass-flow controllers. The composition of the reaction mixture was monitored by an online gas chromatogram equipped with an FID detector coupled with a methanizer. In each measurement, the catalyst contained the same amount (5 mg) of Au nanoparticles. For the supported catalysts prepared by the colloidal deposition method, 0.200 g of the catalysts (2.5 wt% Au) prepared by the colloidal deposition method were used in measurements. For these catalysts, the space velocity was ~15 000 cm^3/(h·g). The heights of the catalyst bed were ~5, 5, and 3 cm and the corresponding contact times were ~7.5, 7.5, and 4.5 s for TiO_2-, SiO_2-, and activated carbon- supported catalysts, respectively. For the TiO_2-supported Au –Fe_3O_4-1 or Au–Fe_3O_4-2 prepared by the thermal decomposition method, the contact time was estimated to be 0.8 s. To examine whether there is diffusion limitation in our measurements, the as-prepared catalysts were also mixed with different amounts of quartz sand for catalysis measurements. However, the reactivities of the catalysts mixed with quartz sand were identical to those of the corresponding as-prepared catalysts. We can therefore assume the absence of any diffusion limitations on the overall reactivity of the catalysts.

2. Results and discussion

Figure 1 shows two types of Au–Fe_3O_4 dumbbell nano-heterojunction particles prepared in our studies. While the gold nanoparticles in both types had the same size around 6.7 nm, the Fe_3O_4 nanoparticles intergrown with the Au nanoparticles were of different size, namely, 15.2 and 4.9 nm. The as-prepared dumbbell particles with 15.2 and 4.9 nm Fe_3O_4 nanoparticles are denoted Au–Fe_3O_4-1 and Au–Fe_3O_4-2, respectively. To prepare these Au–Fe_3O_4 particles, 6.7 nm Au nanoparticles (Fig. 1(a)) were first made in chloroform by reducing $HAuCl_4$ in the presence of OAm by *tert*-butylamine:borane complex,

a reducing agent that was used recently for the preparation of monodisperse Au nanoparticles [25, 26]. These pre-made Au nanoparticles were separated and transferred into a mixed solution of OLA and OAm containing $Fe(acac)_3$. $Fe(acac)_3$ and $Fe(CO)_5$ have both previously been used as the precursors to make Au–Fe_3O_4 dumbbell nanoparticles [27, 28]. In our studies, $Fe(acac)_3$ rather than $Fe(CO)_5$ was selected as the Fe_3O_4 precursor, because $Fe(CO)_5$ is highly hazardous. The mixture containing Au nanoparticles and $Fe(acac)_3$ was then subjected to heating to allow the growth of Fe_3O_4 nanoparticles on the surface of the Au particles. Conventional heating in a Schlenk tube and microwave heating were both employed in the synthesis of Au–Fe_3O_4-1 (Fig. 1(b)) and Au–Fe_3O_4-2 (Fig. 1(c)), respectively. By using conventional heating, a high temperature (300 °C), was required to produce Au–Fe_3O_4-1 particles. It
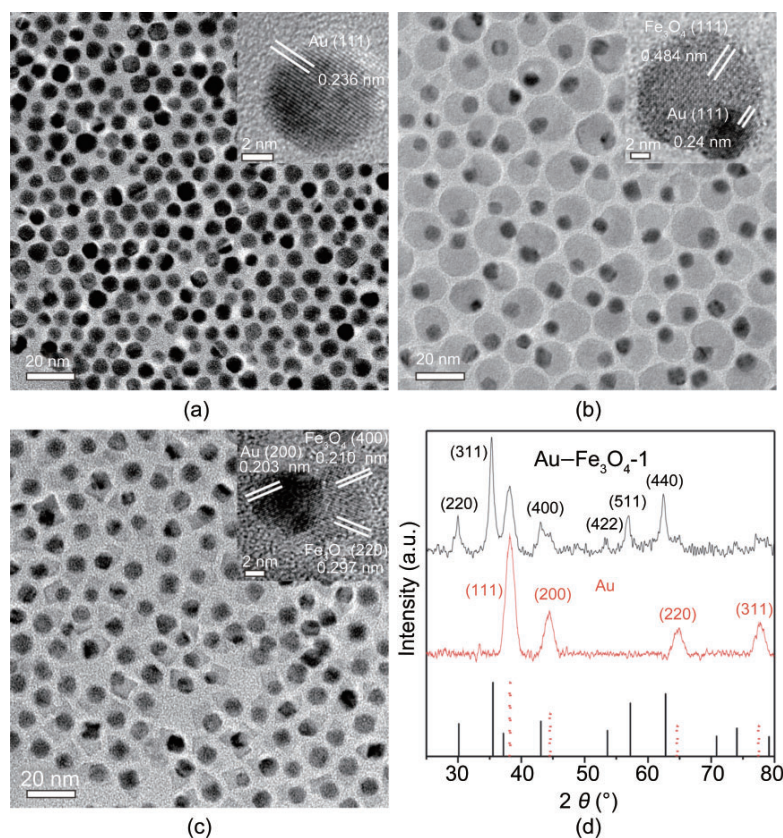

(a)

(b)

(c)

(d)

Figure 1 TEM and HRTEM images of (a) the 6.7 nm Au nanoparticles, (b) Au (6.7 nm)–Fe_3O_4 (15.2 nm) dumbbell nanoparticles prepared by conventional heating, and (c) Au (6.7 nm)–Fe_3O_4 (4.9 nm) dumbbell nanoparticles prepared by microwave heating. (d) Powder XRD patterns of as-prepared 6.7 nm Au and Au (6.7 nm)–Fe_3O_4 (15.2 nm). The standard peaks of Au and Fe_3O_4 are shown at the bottom of the figure by dotted and solid lines, respectively

should also be pointed out that in terms of ensuring that most Au particles formed hybrid particles, it was difficult to prepare Au–Fe$_3$O$_4$ dumbbell particles having smaller Fe$_3$O$_4$ particles by conventional heating. We believe that using smaller sized Fe$_3$O$_4$ particles in Au–Fe$_3$O$_4$ hybrid particles will reduce steric hindrance allowing the Au nanoparticles in dumbbell particles to make better contact with other support materials. this will be discussed later in this article. It is important to note, therefore, that by using microwave heating—a much more efficient form of heating—we have successfully synthesized Au–Fe$_3$O$_4$-2 particles having small Fe$_3$O$_4$ particles with a size of just 4.9 nm at a lower temperature (185 °C).

The inset of Fig. 1(b) shows a typical HRTEM image of an individual Au–Fe$_3$O$_4$-1 particle. Lattice fringes were clearly observed in both Au and Fe$_3$O$_4$ parts of the dumbbell particle. The distance between two adjacent planes in Fe$_3$O$_4$ was measured to be 0.484 nm, corresponding to (111) planes in the inverse spinel structured Fe$_3$O$_4$ and that in Au was 0.236 nm, resulting from the (111) planes in fcc Au. This result is consistent with the suggestion that the facile preparation of Au–Fe$_3$O$_4$ heterostructures is a result of the small lattice mismatch (~2.5%) between 2d$_{111}$-(Au) and d$_{111}$-(Fe$_3$O$_4$) [27, 28]. The power XRD

pattern (Fig. 1(d)) of the as-prepared bulk Au–Fe$_3$O$_4$-1 sample also confirmed the inverse spinel structure of Fe$_3$O$_4$ and the fcc structure of Au in the as-prepared dumbbell particles. The direct growth of the Fe$_3$O$_4$ on the Au nanoparticles is likely to reduce the mobility of Au nanoparticles and therefore prevent their facile aggregation during reactions or thermal treatments.

To support the hypothesis that the intergrowth in Au–Fe$_3$O$_4$ would help to stabilize the Au nanoparticles against aggregation, we performed comparative studies of 6.7 nm Au nanoparticles alone and Au–Fe$_3$O$_4$-1 dumbbell nanoparticles containing 6.7 nm Au nanoparticles. Both Au and Au–Fe$_3$O$_4$-1 were deposited on supports through the colloidal deposition method [23, 24]. The method allows the preparation of well-defined nanocatalysts from as-made nanoparticles, which can be hydrophobic. The deposition of organic-passivated Au and Au–Fe$_3$O$_4$-1 nanoparticles on Degussa P25 TiO$_2$ was carried out in chloroform. The as-deposited composites were catalytically inactive before any thermal treatment. Both Au and Au–Fe$_3$O$_4$-1 composites with TiO$_2$ were then calcined at 350, 450, or 550 °C to remove the organic species. As shown in Fig. 2, the sintering of Au nanoparticles in the Au/TiO$_2$ composite was evidenced by the formation of large Au particles
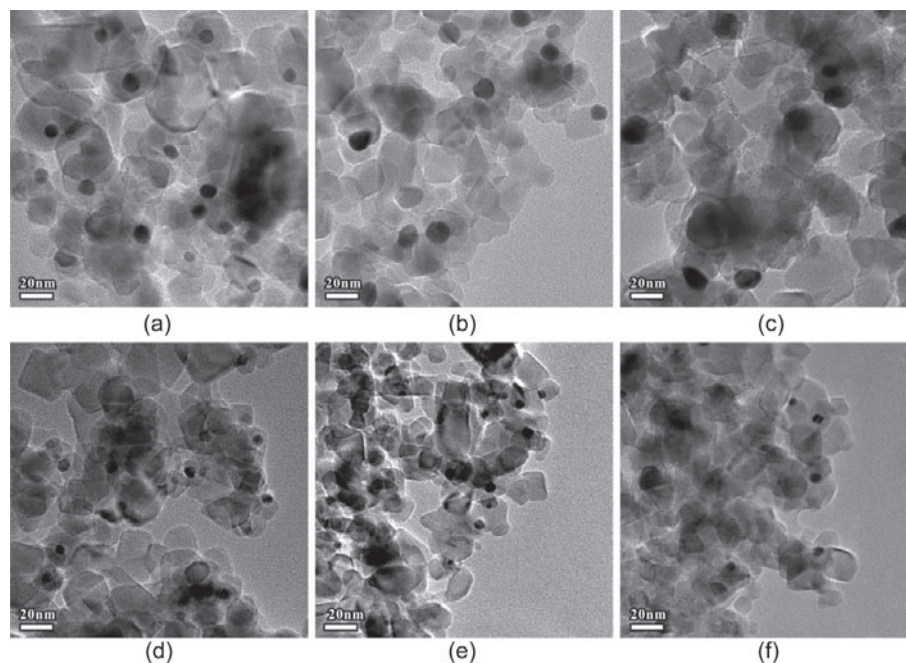

Figure 2   TEM images of Au/P25 TiO$_2$ calcined at (a) 350 °C, (b) 450 °C, and (c) 550 °C, and Au–Fe$_3$O$_4$-1/P25 TiO$_2$ calcined at (d) 350 °C, (e) 450 °C, and (f) 550 °C

(as large as 30 nm). As expected, when Au–Fe$_3$O$_4$ nanoparticles were dispersed on TiO$_2$, however, the Au particles retained their original size even after thermal treatment at 550 °C, suggesting that the dumbbell intergrowth structure results in a marked stabilization of the Au nanoparticles against sintering.

A similar stabilizing effect was also observed when Au–Fe$_3$O$_4$-1 particles were supported on SiO$_2$ or activated carbon. No sintering of the Au nanoparticles was observed, neither in SiO$_2$- nor in activated carbon-supported Au–Fe$_3$O$_4$-1 treated at 450 °C. Although the size of the Au nanoparticles was kept the same in all SiO$_2$-, TiO$_2$-, and C-supported Au–Fe$_3$O$_4$-1, they performed differently in the catalytic oxidation of CO as shown in their light-off curves (Fig. 3(c)). While carbon-supported Au–Fe$_3$O$_4$-1 displayed negligible activity, TiO$_2$-supported Au–Fe$_3$O$_4$-1 exhibited the best performance of the three supported catalysts, indicating a significant support effect on the activity of supported Au–Fe$_3$O$_4$-1. It is worth mentioning that when Au–Fe$_3$O$_4$-1 itself was calcined at 450 °C, it showed no catalytic activity for CO oxidation. These results are in remarkable contrast to what has been previously observed for the Au–Fe$_3$O$_4$ dumbbell particles having 3 nm Au nanoparticles, which easily achieved 100% CO conversion at temperatures lower than 60 °C, with or without any other support [24]. According to the size-dependent studies by Haruta and Goodman [1–3, 5, 29], the activity of supported Au nanoparticles should sharply decrease when their size is above 6 nm. Our results were reasonably consistent with such a size model.

Together with their lack of catalytic activity, the capability of stabilizing Au nanoparticles against sintering makes the dumbbell Au–Fe$_3$O$_4$ particles having 6.7 nm Au nanoparticles an excellent system to study the support effect without there being any possible influence from the size effect. Based on the above support-dependent studies, we propose that the built-in Au–TiO$_2$ interface is essential

to activate the dumbbell Au–Fe$_3$O$_4$ particles having 6.7 nm Au nanoparticles for CO oxidation. The importance of the Au–TiO$_2$ interface is further supported by comparison of TiO$_2$-supported Au–Fe$_3$O$_4$-1 samples calcined at different temperatures (350, 450, and 550 °C). While the size of Au nanoparticles remained the same, the catalytic activity of the TiO$_2$-supported materials decreased with calcination temperature (Fig. 3(d)). This result can be reasonably explained by the higher degree of Au–TiO$_2$ interface breakage at higher calcination temperature.

Since the catalytic activity of TiO$_2$-supported Au–Fe$_3$O$_4$-1 was correlated with the Au–TiO$_2$ interface, this suggested the possibility of enhancing the catalytic performance of Au–Fe$_3$O$_4$-1 particles by enlarging the Au–TiO$_2$ interface. To maximize the interfacial contact between the Au nanoparticles in Au–Fe$_3$O$_4$-1 and TiO$_2$, we attempted to introduce TiO$_2$ by the *in situ* thermal decomposition of a precursor (TIPO). Following the thermal decomposition, the as-made TiO$_2$–Au
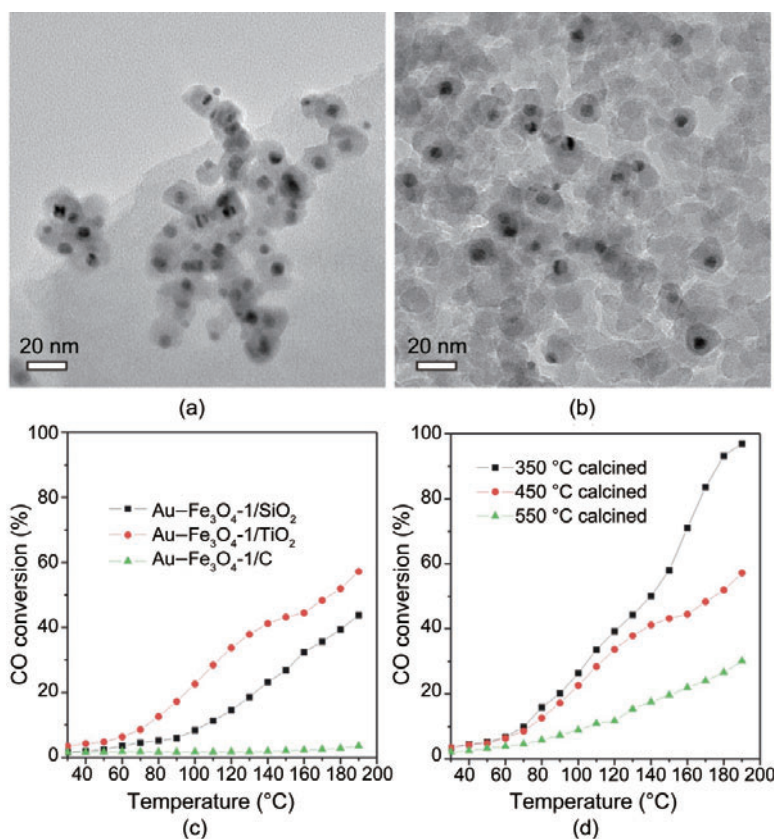

Figure 3 TEM images of (a) activated carbon- and (b) SiO$_2$-supported Au–Fe$_3$O$_4$-1 (calcined at 450 °C). CO oxidation conversion light-off curves of the Au nanocatalysts (c) with different supports (calcined at 450°C) and (d) supported on P25 TiO$_2$ with different treatment temperatures

–Fe$_3$O$_4$-1 composites were subjected to thermal treatments at 350, 450, and 550 °C. As illustrated in Figs. 4(a)–4(c), again no aggregate growth of the Au nanoparticles was observed in the all cases, confirming the stabilizing effect conferred by the intergrowth between Au and Fe$_3$O$_4$ in the dumbbell structure. The TEM images also clearly show that the particle size of TiO$_2$ increased with the thermal treatment temperature. Based on the TEM observations, the sample treated at 350°C should have the maximum Au–TiO$_2$ interfacial contact and therefore the best catalytic performance in CO oxidation. The catalytic tests, however, showed that the composites treated at 450 °C showed the best activity (Fig. 4(d)). Although our XRD studies also confirmed the increase in anatase TiO$_2$ crystallite size with treatment temperature (Fig. 4(e)), the TGA curve (Fig. 4(f)) for the as-prepared untreated TiO$_2$–Au–Fe$_3$O$_4$-1 composites revealed that a large amount of organic residue remained when the sample was treated at 350 °C. OLA present during

the thermal decomposition might account for such organic residues. Undoubtedly, the presence of organic species on the TiO$_2$ surface was deleterious to the effective contact of the Au nanoparticles with TiO$_2$ and therefore to the overall catalytic performance of the composites. In contrast to thermal treatment at 350 °C, treatment at 450 °C for 2 h in air completely removed the organic residues and resulted in good Au–TiO$_2$ contact. When further thermally treated at 550 °C, TiO$_2$ grew into larger particles, leading to the loss of the Au–TiO$_2$ interface. Therefore, the fact that the catalytic performance of the composites treated at 450 °C was better than that of those treated at either 350 or 550° C can be nicely explained in the term of the Au–TiO$_2$ interfacial contact. Importantly, the thermal deposition of TiO$_2$ precursors was found more effective than colloidal decomposition in creating an Au–TiO$_2$ interface on the Au–Fe$_3$O$_4$ dumbbell particles.

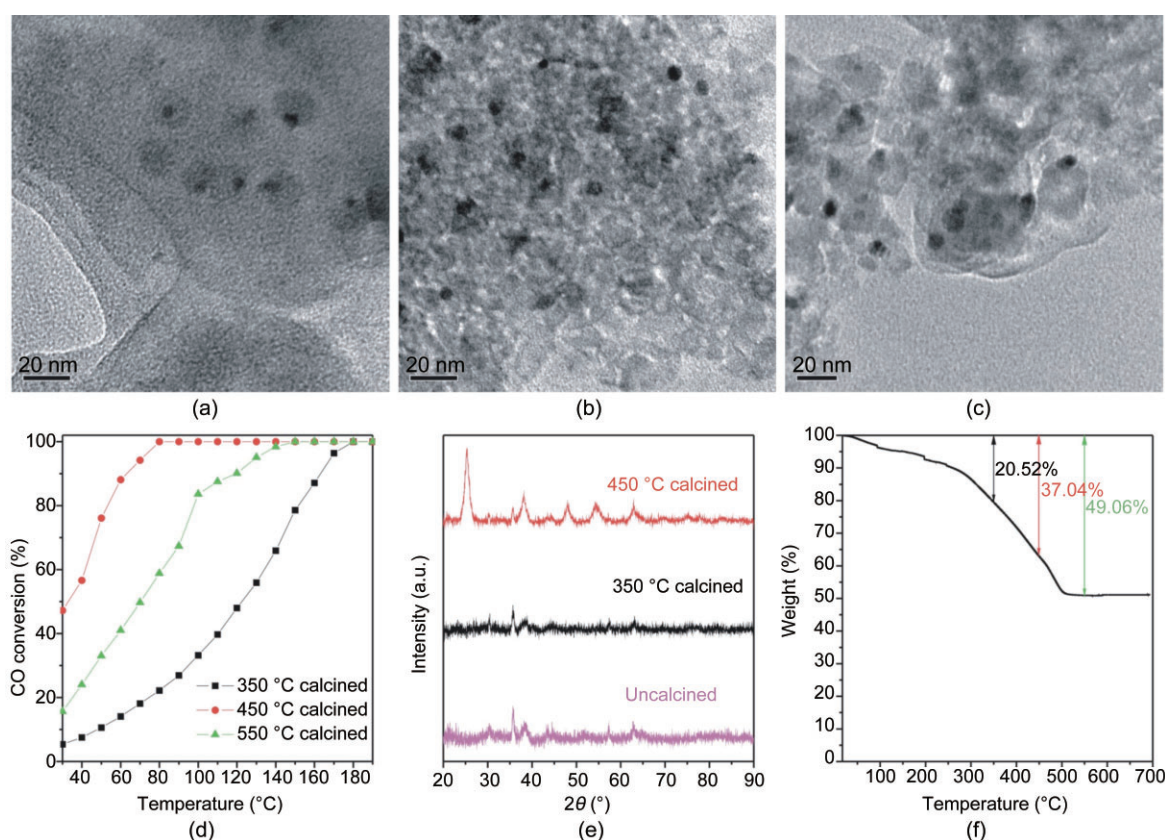While all the observations discussed above support the importance of the Au–TiO$_2$ interface in

Figure 4 TEM images of Au–Fe$_3$O$_4$-1/TiO$_2$ prepared by *in situ* thermal decomposition of 0.6 mL TIPO and calcined at (a) 350 °C, (b) 450 °C, and (c) 550 °C. (d) CO oxidation conversion light-off curves of the Au–Fe$_3$O$_4$-1/TiO$_2$ nanocatalysts shown in (a)–(c). (e) XRD pattern of Au–Fe$_3$O$_4$/TiO$_2$ prepared by thermal decomposition and calcined at different temperatures. (f) TGA curve of Au–Fe$_3$O$_4$-1/TiO$_2$ catalyst prepared by thermal decomposition of 0.6 mL TIPO and dried at 100 °C

activating Au–Fe$_3$O$_4$ dumbbell particles having 6.7 nm Au nanoparticles for CO oxidation, we have found difficulty in converting Au–Fe$_3$O$_4$-1 particles into catalysts that are as efficient as supported Au nanoparticles having a smaller size. The main factor hindering us in achieving this is the large size of the Fe$_3$O$_4$ particles in Au–Fe$_3$O$_4$-1 which results in significant steric hindrance to contact between Au nanoparticles and TiO$_2$ in the dumbbell particles. To resolve this steric problem, it is desirable to make dumbbell particles containing smaller Fe$_3$O$_4$ nanoparticles. As discussed above, microwave heating has helped to achieve the synthesis of such dumbbell particles (Au–Fe$_3$O$_4$-2) having 4.9 nm Fe$_3$O$_4$ nanoparticles. As shown in Fig. 5(a), when Au–Fe$_3$O$_4$-2 was thermally treated with 20 μL of TIPO under microwave heating followed by calcination at 350 °C, the size of Au particles was maintained. Au–Fe$_3$O$_4$-2 was also highly dispersed on TiO$_2$. The as-prepared catalysts exhibited high catalytic activity of CO oxidation at 30 °C with 100% CO conversion (Fig. 5(b)). Therefore, the TiO$_2$-supported Au–Fe$_3$O$_4$-2 particles have both high catalytic activity and high stability. No decline in the catalytic performance of the calcined TiO$_2$–Au–Fe$_3$O$_4$-2 was observed up to 6 h. In comparison, the activated carbon-supported Au–Fe$_3$O$_4$-2 calcined at 350 °C exhibited much lower activity. However, compared with Au–Fe$_3$O$_4$-1, Au–Fe$_3$O$_4$-2 supported on activated carbon displayed an improved catalytic performance. Therefore, at this point, even though we can confirm the important role of the smaller size of Fe$_3$O$_4$ nanoparticles in enlarging
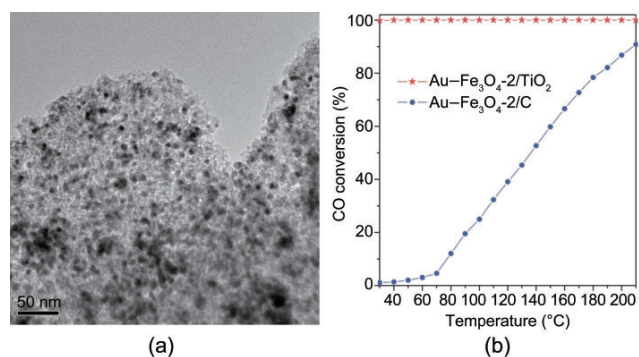
the Au–TiO$_2$ contact (Fig. S-1), it is not possible to exclude a contribution from the morphology and size of the Fe$_3$O$_4$ nanoparticles to the overall catalytic performance of TiO$_2$–Au–Fe$_3$O$_4$-2. Further work is now in progress to elucidate the effect of the morphology and size of Fe$_3$O$_4$ in Au–Fe$_3$O$_4$ hybrid nanoparticles on their catalytic performance.

3. Conclusions

Au (6.7 nm)–Fe$_3$O$_4$ dumbbell nanoparticles have been demonstrated to be an excellent system to study the Au metal–oxide support effect without any possible influence of the size effect of Au. Using Au (6.7 nm)–Fe$_3$O$_4$ dumbbell nanoparticles as the precursors for catalyst preparation, we have revealed the importance of the Au–TiO$_2$ interface in CO oxidation. The Au–TiO$_2$ interface was increased by depositing TiO$_2$ on Au–Fe$_3$O$_4$ by *in situ* thermal decomposition of TiO$_2$ precursors, which helped to optimize the catalytic performance by supported Au–Fe$_3$O$_4$ particles. By utilizing the Au–TiO$_2$ support effect, the catalytically inert Au (6.7 nm)–Fe$_3$O$_4$ dumbbell nanoparticles can be converted into catalysts which are highly efficient for CO oxidation at room temperature.

Acknowledgements

Electronic Supplementary Material: Supplementary material is available in the online version of this article at http://dx.doi.org/10.1007/s12274-009-9102-z and is accessible free of charge.

Figure 5 (a) TEM image of Au–Fe$_3$O$_4$-2/TiO$_2$ prepared by thermal decomposition under microwave irradiation and calcined at 350 °C. (b) CO oxidation conversion light-off curves of the Au–Fe$_3$O$_4$-2/TiO$_2$ nanocatalyst shown in (a) and activated carbon-supported Au–Fe$_3$O$_4$-2 calcined at 350 °C

References

[1] Haruta, M. Catalysis of gold nanoparticles deposited on

metal oxides. *Cattech* **2002**, *6,* 102–115.

[2] Haruta, M. When gold is not noble: Catalysis by nanoparticles. *Chem. Rec.* **2003**, *3, 75*–87.

[3] Haruta, M. Gold as a novel catalyst in the 21st century: Preparation, working mechanism and applications. *Gold Bull.* **2004**, *37,* 27–36.

[4] Bond, G. C.; Thompson, D. T. Catalysis by gold. *Catal. Rev. -Sci. Eng.* **1999**, *41,* 319–388.

[5] Chen, M. S.; Goodman, D. W. The structure of catalytically active gold on titania. *Science* **2004**, *306,* 252–255.

[6] Hughes, M. D.; Xu, Y. J.; Jenkins, P.; McMorn, P.; Landon, P.; Enache, D. I.; Carley, A. F.; Attard, G. A.; Hutchings, G. J.; King, F. et al. Tunable gold catalysts for selective hydrocarbon oxidation under mild conditions. *Nature* **2005**, *437,* 1132–1135.

[7] Hashmi, A. S. K.; Hutchings, G. J. Gold catalysis. *Angew. Chem. Int. Ed.* **2006**, *45,* 7896–7936.

[8] Corma, A.; Garcia, H. Supported gold nanoparticles as catalysts for organic reactions. *Chem. Soc. Rev.* **2008**, *37*, 2096–2126.

[9] Corma, A.; Serna, P. Chemoselective hydrogenation of nitro compounds with supported gold catalysts. *Science* **2006**, *313,* 332–334.

[10] Grirrane, A.; Corma, A.; Garcia, H. Gold-catalyzed synthesis of aromatic azo compounds from anilines and nitroaromatics. *Science* **2008**, *322,* 1661–1664.

[11] Turner, M.; Golovko, V. B.; Vaughan, O. P. H.; Abdulkin, P.; Berenguer-Murcia, A.; Tikhov, M. S.; Johnson, B. F. G.; Lambert, R. M. Selective oxidation with dioxygen by gold nanoparticle catalysts derived from 55-atom clusters. *Nature* **2008**, *454,* 981–983.

[12] Haruta, M.; Kobayashi, T.; Sano, H.; Yamada, N. Novel gold catalysts for the oxidation of carbon monoxide at a temperature far below 0 °C. *Chem. Lett.* **1987**, *16,* 405–408.

[13] Haruta, M.; Yamada, N.; Kobayashi, T.; Iijima, S. Gold catalysts prepared by coprecipitation for low-temperature oxidation of hydrogen and of carbon monoxide. *J. Catal.* **1989**, *115,* 301–309.

[14] Haruta, M. Size- and support-dependency in the catalysis of gold. *Catal. Today* **1997**, *36,* 153–166.

[15] Ma, Z.; Overbury, S. H.; Dai, S. Au/M$_x$O$_y$/TiO$_2$ catalysts for CO oxidation: Promotional effect of main-group, transition, and rare-earth metal oxide additives. *J. Mol. Catal. A-Chem.* **2007**, *273,* 186–197.

[16] Comotti, M.; Li, W. C.; Spliethoff, B.; Schuth, F. Support effect in high activity gold catalysts for CO oxidation. *J. Am. Chem. Soc.* **2006**, *128,* 917–924.

[17] Iizuka, Y.; Tode, T.; Takao, T.; Yatsu, K.; Takeuchi, T.; Tsubota, S.; Haruta, M. A kinetic and adsorption study of CO oxidation over unsupported fine gold powder and over gold supported on titanium dioxide. *J. Catal.* **1999**, *187,* 50–58.

[18] Schwartz, V.; Mullins, D. R.; Yan, W. F.; Chen, B.; Dai, S.; Overbury, S. H. XAS study of Au supported on TiO$_2$: Influence of oxidation state and particle size on catalytic activity. *J. Phys. Chem. B* **2004**, *108,* 15782–15790.

[19] Beck, A.; Horvath, A.; Stefler, G.; Scurrell, M. S.; Guczi, L. Role of preparation techniques in the activity of Au/TiO$_2$ nanostructures stabilised on SiO$_2$: CO and preferential CO oxidation. *Top. Catal.* **2009**, *52,* 912–919.

[20] Soares, J. M. C.; Bowker, M. Low temperature CO oxidation on supported and unsupported gold compounds. *Appl. Catal. A-Gen.* **2005**, *291,* 136–144.

[21] Grunwaldt, J. D.; Kiener, C.; Wogerbauer, C.; Baiker, A. Preparation of supported gold catalysts for low-temperature CO oxidation via "size-controlled" gold colloids. *J. Catal.* **1999**, *181,* 223–232.

[22] Chou, J.; McFarland, E. W. Direct propylene epoxidation on chemically reduced Au nanoparticles supported on titania. *Chem. Commun.* **2004**, 1648–1649.

[23] Zheng, N.; Stucky, G. D. A general synthetic strategy for oxide-supported metal nanoparticle catalysts. *J. Am. Chem. Soc.* **2006**, *128,* 14278–14280.

[24] Yin, H. F.; Wang, C.; Zhu, H. G.; Overbury, S. H.; Sun, S. H.; Dai, S. Colloidal deposition synthesis of supported gold nanocatalysts based on Au–Fe$_3$O$_4$ dumbbell nanoparticles. *Chem. Commun.* **2008**, 4357–4359.

[25] Peng, S.; Lee, Y.; Wang, C.; Yin, H.; Dai, S.; Sun, S. A facile synthesis of monodisperse Au nanoparticles and their catalysis of CO oxidation. *Nano Res.* **2008**, *1,* 229–234.

[26] Zheng, N.; Fan, J.; Stucky, G. D. One-step one-phase synthesis of monodisperse noble-metallic nanoparticles and their colloidal crystals. *J. Am. Chem. Soc.* **2006**, *128,* 6550–6551.

[27] Shi, W.; Zeng, H.; Sahoo, Y.; Ohulchanskyy, T. Y.; Ding, Y.; Wang, Z. L.; Swihart, M.; Prasad, P. N. A general approach to binary and ternary hybrid nanocrystals. *Nano Lett.* **2006**, *6,* 875–881.

[28] Yu, H.; Chen, M.; Rice, P. M.; Wang, S. X.; White, R. L.; Sun, S. Dumbbell-like bifunctional Au–Fe$_3$O$_4$ nanoparticles. *Nano Lett.* **2005**, *5,* 379–382.

[29] Chen, M. S.; Goodman, D. W. Catalytically active gold: From nanoparticles to ultrathin films. *Acc. Chem. Res.* **2006**, *39,* 739–746.